NJC

Accepted Manuscript

This article can be cited before page numbers have been issued, to do this please use: S. Kuo, C. LIU, R. Balamurugan, Y. Zhang, S. Fitriyani and J. Liu, *New J. Chem.*, 2017, DOI: 10.1039/C7NJ03059B.

ROYAL SOCIETY OF CHEMISTRY

rsc.li/njc

Dynamic Article Links ►
View Article Online
DOI: 10.1039/C7NJ03059B

Cite this: DOI: 10.1039/c0xx00000x

www.rsc.org/xxxxxx

ARTICLE TYPE

Dual-responsive ALS-type organogelators based on azobenzene-cholesteryl conjugates and their self-assemblies

Sheng-Yang Kuo[1], Chun-Yen Liu[2], Rathinam Balamurugan[1], Yan-Song Zhang[1], Sri Fitriyani[1] and Jui Hsiang Liu[1]*

[1] *Department of Chemical Engineering, National Cheng Kung University, Tainan70101, Taiwan, Republic of China*. Fax: +886-6- 2384590; Tel: +886-6-2757575ext.62646 Corresponding author E-mail: jhliu@mail.ncku.edu.tw

[2] *School of Optometry and Vision Science Program, UC Berkeley, Berkeley, CA 94720, USA*

Received (in XXX, XXX) Xth XXXXXXXXX 20XX, Accepted Xth XXXXXXXXX 20XX
DOI: 10.1039/b000000x

Two structurally isomeric azobenzene- and cholesteryl-based derivatives with varying alkyl chain lengths were developed as ALS-type gelators (N2 and N4) and synthesized and characterized spectroscopically. Of the two, N4 acted as a more efficient gelator than N2 since N4 could gel a larger number of solvents. The critical gelation concentration (CGC) of N4 was found to be less than that of N2 in the same solvent system. The morphological analyses of both gelators using SEM and TEM revealed that N4 exhibited self-assembled fibrous structures, whereas N2 exhibited spherical nanoparticles. The van der Waals interactions between the cholesteryl units, hydrogen bonding between the amide linkages and π-π stacking between the azobenzene units provided the driving force for the aggregation and gel formation. These driving forces were evidenced by temperature dependent ^{1}H-NMR, FTIR and XRD analyses. Increasing the temperature of the gels shifted (upfield and downfield) the protons in the ^{1}H-NMR spectra as well as the absorption bands in the FTIR spectra indicating that the intermolecular forces between the molecules became disrupted and caused *gel→ sol* transitions. These transitions were reversible after cooling to room temperature. Similarly, the *gel→ sol* transitions could be triggered by UV light (due to *trans*/*cis* isomerization); however, the transition was irreversible in the presence of visible light due to the formation of the more stable *cis* isomer. Hence, the gel state could be retained by heating and cooling the *cis*-conformation. In addition, the length of the molecule as determined by simulation software was found to match the values observed from the XRD analysis, and the interlayer distances were found to be 1.78 and 1.85 nm for N2 and N4, respectively. Based on this evidence, an aggregation mechanism was proposed. The differential scanning calorimetry (DSC) and polarized optical microscopy (POM) results revealed that both gelators exhibited grainy nematic mesophase textures during the heating and cooling cycles. These gelators underwent phase-selective gelation in the solvent mixtures containing gelling and nongelling solvents, which demonstrated the applicability of these gelators for the separation and purification of solvents.

Introduction

Organogelators self-assemble into 3D network structures via nonchemical bonding interactions and supramolecular weak interactions, such as van der Waals forces, π-π stacking, hydrogen bonding (H-bonding), electrostatic attractions, metal coordination and hydrophobic interactions[1-10]. These weak interactions can be tuned by temperature, light, pH and mechanical forces. Therefore, organogelators have received increased attention due to their potential applications in light harvesting[11, 12], photovoltaics[13, 14], wound healing[15] and dye-sensitized solar cells[16]. By adding photochromic molecules, such as azobenzene, into the gel, the gel-sol transitions can be controlled by light[17-25]. In particular, cholesterol-based photoresponsive organogelators have attracted a great deal of interest due to their unique properties related to their molecular rigidity, aggregation, asymmetry, and other features[26-35]. Many research groups have developed azobenzene-based

View Article Online
DOI: 10.1039/C7NJ03059B

photoresponsive organogelators both with and without cholesteryl terminal groups, in which the sol-gel transitions are triggered by UV and visible light irradiation that disrupts the intermolecular interactions[8, 18, 20, 24, 25, 36-53]. Cholesteryl based organogelators are classified as ALS, $A(LS)_2$, LS and LS_2, where A refers to the aromatic units that facilitate π-π stacking; L refers to the linker, usually amides/carbamates, which facilitate H-bonding; and S refers to the steroid units, which are generally sugars.[1] Depending on the selection of A, L and S, the aggregation can be regulated. Recently, we reported bis-cholesteryl-appended isosorbide-based organogelators, and their aggregation mechanism was studied[30]. Isosorbide gelators also form gel emulsions with styrene in water/oil (W/O) mixtures suggesting that these gelators can be used as stabilizers for the preparation of monoliths. In addition, we also studied the structure-property relationships of symmetrical and asymmetrical azobenzene-based $(ALS)_2$-type organogelators, and their aggregation phenomena were compared by exchanging the terminal groups with cholesteryl or adamantly groups[54]. We also developed pyridine-cholesteryl based organogelators, and their aggregation and structure-property relationships were studied with respect to substitution effects (ortho and para substitution effects)[55].

In this study, we report azobenzene and cholesteryl-based ALS-type organogelators (N2 and N4), and their gelation and aggregation phenomena were studied with respect to the length of their alkyl chains. These gelators are structurally distinguished by the lengths of the alkyl linkers (ethyl or butyl) between the cholestery and azobenzene units. The terminal cholestery unit, amide linkages and azobenzene are expected to participate in van der Waals interactions, H-bonding and π-π stacking, which lead to gel formation. The gels are thermally reversible, whereas UV light irradiation causes only gel→ sol transitions that are not reversible under visible light. However, the solution can be returned to the gel state by subsequent heating and cooling processes. Moreover, the mesomorphic behaviors of the synthesized gelators were studied with the help of DSC and POM analyses. The application of these gelators for the separation of organic solvents was studied by exploiting the phase-selective gelation ability of the synthesized gelators.

Experimental

Instruments

All chemicals were purchased from Aldrich Chemicals and used without further purification. All solvents were purified before use. Fourier transform infrared spectra (FTIR) were recorded using a Jasco VALOR III Fourier transform infrared spectrophotometer. Nuclear magnetic resonance (NMR) spectra were obtained using a Bruker AMX-400 high-resolution NMR spectrometer (Darmstadt, Germany), and the chemical shifts were reported in ppm with tetramethylsilane (TMS) as the internal standard. The UV/Vis absorption spectra were measured using a Jasco V-550 spectrophotometer. Differential scanning calorimetry (DSC) was conducted using a Perkin-Elmer DSC 7 under a nitrogen atmosphere with heating and cooling rates of 10°C min^{-1}. The sample morphologies were characterized using field-emission scanning electron microscopy (FE-SEM, JSM-7001, JEOL, Japan) and transmission electron microscopy (TEM) with a JEOL JEM-1200CX-II microscope and a Cu-grid substrate. The X-ray diffraction (XRD) measurements of the xerogel were acquired using a Rigaku RINT2000 with a scan rate of 1°/min. The anisotropic properties of the highly ordered and self-assembled samples were investigated using an Olympus BH-2 polarized light microscope (POM) equipped with a Mettler FP-82 hot stage with a temperature scanning rate of 10°C min^{-1}.

Gelation Tests

The gelation abilities of the samples were determined using the heating-cooling-inverting method. For each tested sample, a measured volume of pure organic solvent was added to a known amount of the sample in a sealed glass vial. Next, the solubility of the samples in the solvents at their respective boiling points was studied by heating the vials in a water bath before cooling them to room temperature. Once the solvents cooled to room temperature, they were inverted to check the status of the contents of the vial. The gel state (indicated by immobilization of the solvent) was denoted as "G"; the systems that remained in their solution state were denoted as "S"; the systems in which the samples did not dissolve were denoted as insoluble "I"; and the systems in which the compounds precipitated were referred to as "P". Finally, the minimum concentration of each sample that was required to induce gelation was referred to as the critical gelation concentration "CGC".

Results and Discussion

The cholesteryl-azobenzene conjugate-based organogelators that are structurally isomeric and those with different alkyl chain lengths (spacers) that were used in the current study are shown in Scheme 1. Initially, the cholesteryl chloroformate was reacted with the corresponding diamine (ethylene diamine or butamethylene diamine) in the presence of triethyl amine to afford amine derivatives 2a and 2b. The azobenzene carboxylic acid was synthesized from N,N'-dimethyl aniline and benzoic acid. Finally, the esterification of the amine derivatives with the azobenzene carboxylic acid was conducted using DCC/DMAP[56] to obtain N2 and N4 in moderate yields. The synthetic procedures and the spectroscopic data of the precursors, intermediates and target compounds are provided in the supporting information. All the spectral data for the synthesized intermediates and target compounds corresponded to the structures of the intended compounds.

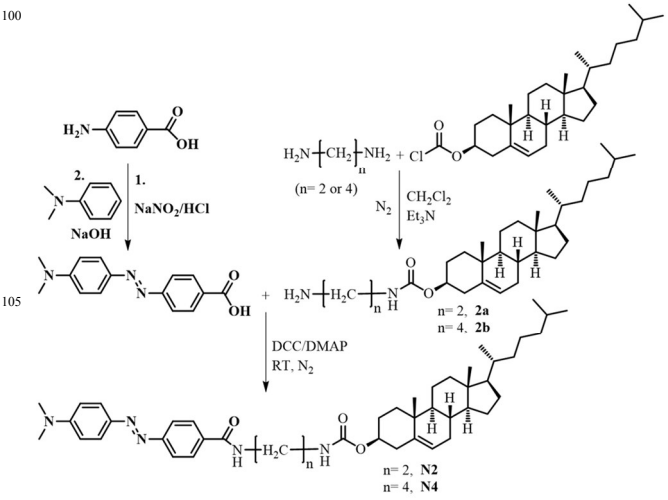

View Article Online
DOI: 10.1039/C7NJ03059B

Scheme 1 Structures of the designed compounds for this organogel system

Gelation & structure-property relationships

The structure-property relationships address the structural features of the gelators, the influences of the solvents and the roles of the noncovalent interactions, gel properties and their spectral data. The gelation abilities of the synthesized N2 and N4 compounds were tested in various organic solvents, and the results are summarized in **Table 1**. Both N2 and N4 form gels in particular solvents. As shown in the table, N4 forms gels in more solvents (6 solvents) than N2 (2 solvents), suggesting that N4 acts as a more versatile gelator than N2. Structurally, N2 and N4 only differ in the lengths of their alkyl chains between their aromatic and cholesteryl units. Therefore, the difference in the gelation abilities between N2 and N4 may be due to the difference in the length of the flexible alkyl chains (spacer lengths) between the aromatic and cholesteryl units, suggesting that the spacer length is crucial for the gel formation. In our earlier report[30, 55, 57], we found that azobenzene derivatives with either no alkyl chains or short alkyl chains (<6 carbons) acted as more efficient gelators compared to their long-chain azobenzene derivatives. Moreover, the CGC value for N4 was found to be lower than that of N2; for example, the CGC of N2 is 20 gL^{-1}, whereas the CGC of N4 is only 10 gL^{-1}. These results indicate that the ethylene chain does not sufficiently improve gelation. This result may be due to the sterically hindered fragments, such as the cholesteryl groups, affecting the intermolecular H-bonding between the amides.

Table 1 Gelation properties of the representative compounds in various solvents

Solvents/Compound	N2	N4
Water	I [a]	I
Methanol	I	I
Ethanol	P	P
1-Propanol	P	P
2-Propanol	P	P
1-Butanol	P	P
2-Butanol	P	P
1,4 Butandiol	P	I
Octanol	P	G (15)[b]
1-Docdcanol	P	P
Cyclopentanone	P	S
1,4-Dioxane	P	P
DMSO	P	G (2.5)
Anisole	P	S
Benzene	P	P
DMF	P	P
Cyclohexane	S	G (10)
Chloroform	S	S
Acetone	S	S
THF	S	S
MEK	S	S
NMP	S	S
Pyridine	S	G (8)
m-Kresol	S	S
Diphenyl ether	G (30)	G (25)
Xylene	G (20)	G (10)

[G=gel; P=precipitate; S=soluble; I=insoluble; CGC values (gL^{-1}) are given parentheses]

Moreover, the cholesteryl groups at the terminal position also have profound effects on gel formation. As shown in the table, N4 forms a gel in 1-octanol; however, it fails to form a gel in 1-dodecanol. Both gelators form gels in diphenyl ether and xylene. N4 can form a gel in pyridine, whereas N2 is dissolved by the same solvent. This result indicates that the nature of the solvent is critical during the gelation process. The gel is opaque reddish orange in all cases, and no remarkable color differences exist between the solvents (**Fig. 1**).

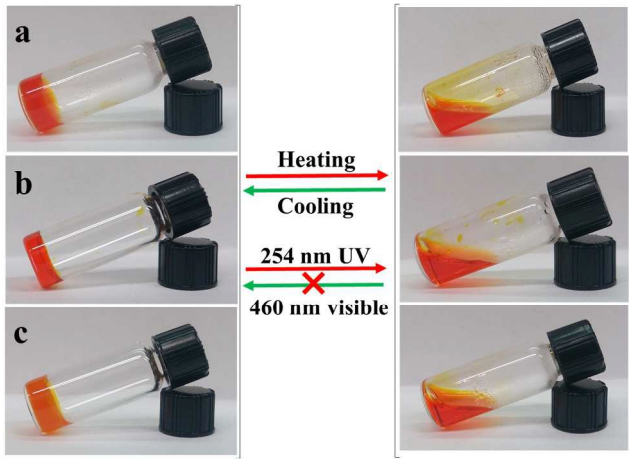

Fig. 1. Sol-gel transition of N2 in xylene (a), N4 in DMSO (b) and N4 in cyclohexane (c) by heating-cooling at the critical gelation concentration. For all cases, the gel→sol transition can be triggered by UV light but cannot be reversed using visible light irradiation.

Morphological studies

To gain visual insight into the morphologies of the molecular aggregation modes, all the gelators were subjected to a TEM analysis, and the results are depicted in **Fig. 2**. As observed in the TEM images, the xerogel of N2 in xylene and diphenyl ether exhibited spherical nanoparticles (2a and b, respectively), whereas N4 exhibited self-assembled, one-dimensional, fiber-like aggregates with lengths of 500 nm and diameters of approximately 100 nm (c and d, respectively). These xerogels undergo further entanglement to form bundles of fibrous aggregates (**Fig. 2a-d**).

View Article Online
DOI: 10.1039/C7NJ03059B

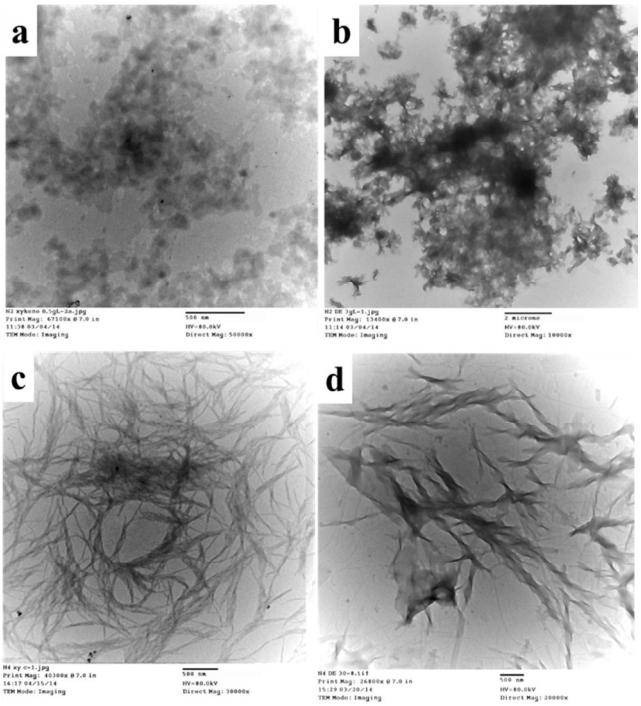

Fig. 2. Representative TEM images of N2 in xylene (a) and diphenyl ether (b) and N4 in xylene (c) and diphenyl ether (d). [Scale Bar: a, c and d: 500 nm; b: 2μm]

Both solvents are low polarity aromatic solvents that may enhance the intermolecular forces, especially π-π stacking, that lead to the formation of gels. The results show that the molecular self-assembly during gel formation is not necessarily fibrous, and if there is sufficient contact area between the molecules, the intermolecular forces will be able to form a gel.

N4 has the lowest critical gel concentration in DMSO, which indicates that N4 exhibits the best gelation ability in that gel system. This result was further supported by the SEM analysis, as shown in **Fig. 3c** and **d**.

The amide bond of the azobenzene can interact with the hydrogen bonds of the DMSO or the hydrogen bonds of the octanol to reduce the intermolecular hydrogen bonding between the amine and the azobenzene so that the van der Waals forces and π-π stacking forces become the main driving forces behind the self-assembly, making the arrangements more regular. TEM can be used to clearly observe the fibrous structure; however, hydrogen bonds cannot form with a solvent such as xylene or diphenyl ether, so the molecular hydrogen bond barrier molecules become stacked, as shown in the TEM image, creating short fibrous structures and causing the minimum critical gel concentration to be relatively high.

This phenomenon is further supported by the gel analysis using ATR spectroscopy; the results of which are shown in **Fig. S5** (Supporting Information). From the figure, the absorption peaks of the carbon-oxygen double bonds (carbonyl group; -C=O) appear at 1703 cm^{-1} and 1687 cm^{-1} in the low polarity solvents (xylene) and the absorption peak at 1689 cm^{-1} in the nonpolar solvent (cyclohexane). The absorption peak of the gels in the polar solvent DMSO is 1700 cm^{-1}. These results indicate that the hydrogen bonds affects the position of the C=O, and the displacement of the peak represents a change in the molecular stacking mode[58, 59].

In most of the azobenzene-cholesteryl-based organogelators, the formation of fibrous aggregate bundles was achieved with noncovalent interactions acting as the driving force for self-assembly. Moreover, in some cases (especially for N4 in diphenyl ether and xylene), twisted helical fibrous structures were observed (**Fig. S6,** Supporting Information) that resulted from the presence of a cholesteryl group, which provided the chiral environment that induced the helical self-assembly. Such twined structures were expected for all the gels but were only observed in a few cases. In most cases, a number of straight fibers were observed. It is possible that the steric hindrance decreased and the free energy increased in the homogeneous fluid solution, as reported by H.C. Lee and Min Li et al[12], or the dense network of entangled fibrils affected the clarity of the structures of the single fiber textures. Moreover, formation of the helical structure also depended upon the sample concentration, type of solvent and sample preparation method. The differences in the morphologies between the different organogels potentially resulted from the different strengths of the hydrophobic interactions between the cholesteryl segments, the π-π stacking and the steric hindrance between the aromatic spacers. All three of these played important roles in regulating the intermolecular orderly stacking and the formation of the twisted fibrous structures[2, 60-72]. We failed to provide SEM images for N2 since no clear images were observed. This may have been due to the agglomeration of nanoparticles, in which the nanoparticles overlapped each other, which could have affected the clarity of the image[73].

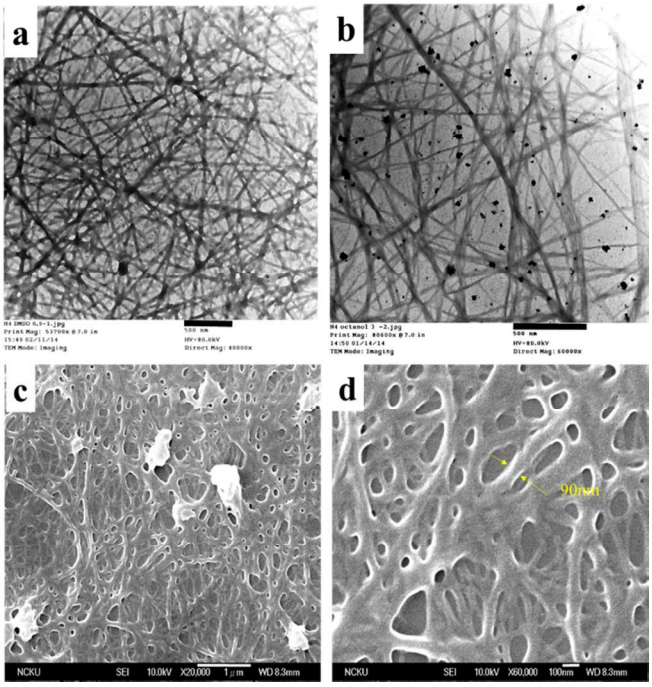

Fig. 3. Representative TEM images of N4 in DMSO (a) and 1-octanol (b) and representative SEM images of N4 in DMSO under different magnifications (c and d) [Scale Bar: a and b: 500 nm; c:1μm; d:100 nm]

View Article Online
DOI: 10.1039/C7NJ03059B

To study the formation and the thermoreversibility of the gels, the temperature-dependency of the ^{1}H-NMR spectra was investigated for N4 in pyridine-d_5 as well as in DMSO-d_6, and the results are presented in **Fig. 4**, **5** and **S7**.

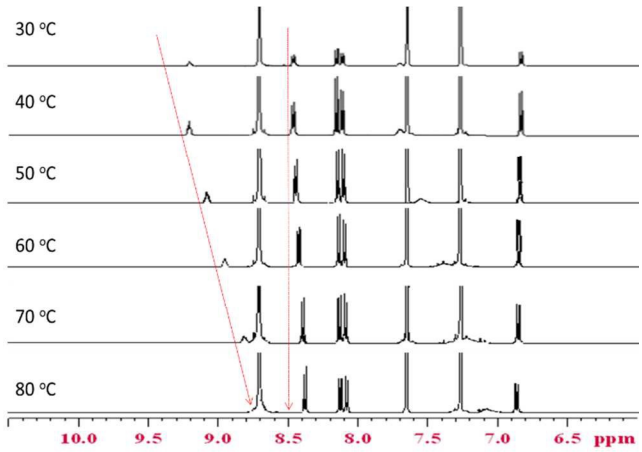

Fig. 4 Temperature-dependent ^{1}H-NMR spectra of the N4/pyridine-d_5 gel over the temperature range of 30 to 80 ℃ from 6-10 ppm.

As observed in the spectra, when the temperature increased from 30 to 80°C, the amide proton [C(=O)-NH-] attached to the benzene ring shifted significantly upfield, from 9.2 ppm to 8.7 ppm. These results indicate that the existence of intermolecular H-bonds was the cause of gel formation at room temperature (30°C). When increasing the temperature from 30 to 80°C, the *gel→sol* transition occurred, which may have been due to the breaking of H-bonds between the molecules, which in turn disrupted the gel state. Increasing the temperature caused disruptions in the supramolecular arrangement and decreased the effects of the secondary forces (the upfield shift was ascribed to the disruption of intermolecular forces between the molecules). This evidence suggested that the intermolecular H-bonding played an important role in the gel formation. Moreover, a downfield shift was also observed for the protons from 0.7 ppm to 0.8 ppm, corresponding to the cholesteryl protons. This results may have been due to the stacking of cholesteryl units (van der Waals forces). The molecular stacking increased the electron density around the protons causing a shielding effect. These van der Waals forces could be disrupted by increasing the temperature. Similar phenomena were observed for the dimethylamine protons attached to the benzene ring, which shifted from 2.9 ppm to 3.0 ppm. In addition, the aromatic protons were found to have shifted upfield from 8.48 ppm to 8.31 ppm, indicating that the benzene rings of the azo fragment were involved in π-π stacking. To summarize the effects of the above forces, it was concluded that van der Waals forces, hydrogen bonding and π-π stacking forces were involved in the molecular self-assembly of these designed gelators; this behavior has been reported in many ALS systems.

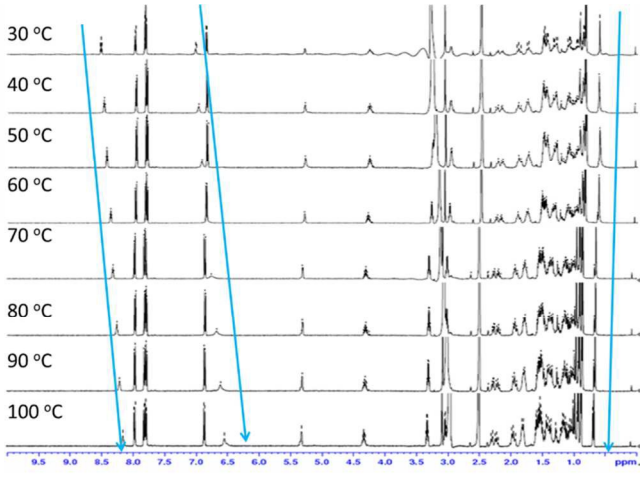

Fig. 5 Temperature dependent ^{1}H-NMR spectra of the N4/DMSO-d_6 gel over a temperature range of 30 to 100 ℃ (from 0-10 ppm).

To gain visual insights into the molecular packing, the xerogels of **N2** and **N4** in xylene were subjected to XRD analysis, and the results are depicted in **Fig. 6**. According to the Bragg lattice diffraction formula, nλ=2d sinθ, where λ is the wavelength and n=1. XRD was used with a copper excitation wavelength of 0.154 nm to determine the incident angle θ and the layer spacing d. Using the data, the formula produced an obvious peak for N2 at 2θ=4.960, and d=1.780. N4 had a peak at 2θ=4.780, and d=1.855 nm. It was also observed that the interlayer distances (spacing) increased with the increasing alkyl chain length (spacer). These interlayer distances were found to coincide with the results obtained from the molecular simulation software (**Fig. 6** inset picture).

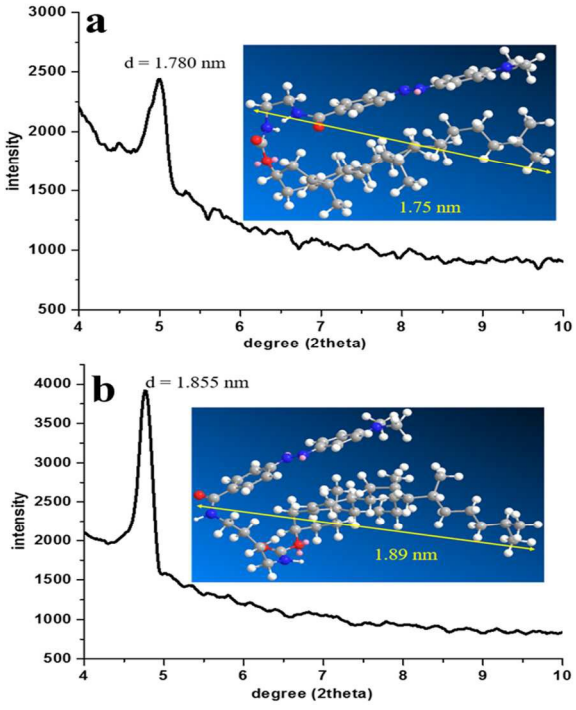

Fig. 6 XRD diffraction patterns and simulated molecular models of (a) N2 and (b) N4.

View Article Online
DOI: 10.1039/C7NJ03059B

Based on the available evidence, it was assumed that the molecule must be folded in order to facilitate the π-π stacking of the azobenzene, the van der Waals interactions between the cholesteryl groups and the H-bonding between the amides and other molecules. The conformation of the folded structure places the amide bond in the backbone of the molecule, and in this arrangement, one end of the amide moiety can act as a hydrogen bond donor to promote molecular assembly. The schematic representation of the molecular assembly facilitated by all the secondary forces is shown in **Fig. 7**.

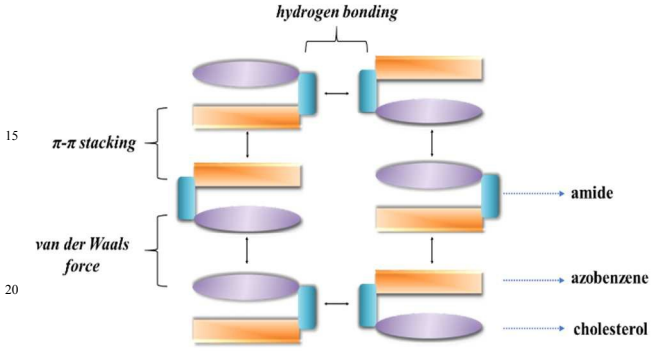

Fig. 7 Schematic representation of the molecular arrangements due to π-π stacking, van der Waals forces and H-bonding for gel formation.

Optical properties of the gelators

The effects of photo-irradiation on the gels were studied by irradiating the gel with UV-Vis light, and the changes were observed. For example, the photolysis of the N2 (0.0375 gL^{-1}) and N4 (0.03 gL^{-1}) gels in DMSO under UV irradiation is shown in **Fig. 8**.

Usually, azobenzene exhibits two absorption peaks at approximately 320 nm and 430 nm that correspond to the π→π* and n→π* transitions indicating *trans-cis* isomerization. However, the absorption spectra of N2 and N4 exhibited broad peaks at 445 nm. This was attributed to the push-pull effect of the dimethylamine and amide groups in N2 and N4, respectively. The functional groups involved in the push-pull of the electron cloud enhanced the HOMO energy level of the azobenzene compound and reduced the LUMO energy level to reduce the bandgap, and the lower energy of the π→π* transition was reflected in the redshift of the absorption wavelength. **Figs. 8a** and **8c** show that the maximum absorbance is in the visible range and exhibits a wider band of absorption wavelengths. In addition, the absorption peak for the n→π* transition is hidden; it cannot be observed because the band overlapped with the much stronger π→π* absorption band.

To further study the photoisomerization mechanism of N2 and N4, the isokinetic reaction rate constants were calculated using the following kinetic formula:

$$-kt = \ln(A\infty - At)/(A\infty - A0)$$

where A0, At, A∞ in the equation represent the intensity of the absorption of ultraviolet light at 254 nm at 0 seconds, t seconds and after infinite time, respectively. Since N2 did not change after 24 minutes of irradiation, A24 was defined as A∞. In addition, the slope of the plot of t (horizontal axis) versus ln $[(A_\infty - A_t) / (A_\infty - A_0)]$ (vertical axis) is equal to -k. The plot of N2 and N4 in DMSO can be divided into two phases, as shown in **Figs. 8b** and **8d**. The linear regression rates were calculated for both segments, and the reaction rate constant of N2 was calculated to be 0.0796 min^{-1} (1.33×10^{-3} s^{-1}) from 0 to 20 minutes and 0.2929 min^{-1} (4.88×10^{-3} s^{-1}) from 20 to 30 minutes; the reaction rate constant of N4 was calculated as 0.1587 min^{-1} (2.65 × 10-3 s^{-1}) from 0 to 14 minutes and 0.1956 min^{-1} (3.26 × 10-3 s^{-1}) from 14 to 24 minutes.

Both gelators (N2 and N4) underwent *trans*→*cis* isomerization after irradiation with UV light. However, after visible light irradiation at a wavelength of 465 nm, the wave pattern remained constant; even if the sample was irradiated for a long time, *cis*→*trans* isomerization did not occur. This results occurred because the amide acts as a hydrogen bond donor to the lone pair of electrons on the azobenzene nitrogen, and the *cis*-azobenzene causes the electron cloud around the nitrogen atom to concentrate on one side to produce a strong bond with the amide. Therefore, in this system, *cis-trans* conformations are more stable, and once the hydrogen bond forms with the trans-azobenzene, it is not easy for the azobenzene to return to the cis conformation. The conformations of N2 and N4 were thermally reversible over repeated heating and cooling cycles; however, the conformations were photoirreversible. Because of the H-bonding between molecules, the stability of *cis*-azobenzene is higher than that of the *trans*-conformation, so it is difficult to revert the molecule to the *trans*-conformation. The network structure of the gel causes light to scatter, and the solution is not transparent. When the small molecules are evenly dispersed, the system becomes transparent.

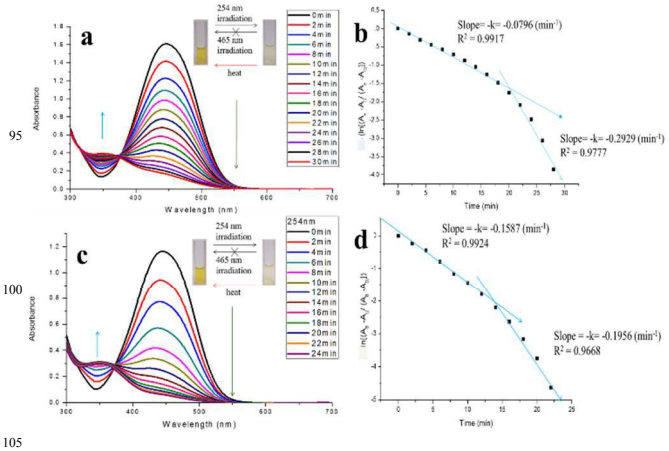

Fig. 8 The dependencies of the UV-Vis spectra (a and c) and ln[$(A_\infty - A_t)/(A_\infty - A_0)$] of N2 (0.03 gL^{-1}) and N4 (0.0375 gL^{-1}) in DMSO (b and d) on the irradiation time with 254 nm light.

Mesomorphic behavior of the gelators

View Article Online
DOI: 10.1039/C7NJ03059B

The thermotropic liquid crystalline properties of the gelators were evaluated using DSC and POM. The POM images and DSC curves of the gelators are shown in **Fig. 9** and **Fig. S8**, respectively. Both the gelators showed well-defined endothermic peaks corresponding to the crystalline transition (T_k: 131 °C for N2 and 132°C for N4), melting transition (T_m: 200°C for N2 and 170°C for N4) and isotropic transition temperatures (T_i: 233°C for N2 and 200°C for N4). The DSC data revealed that the T_m and T_i of the gelators decreased as the flexibility of the methylene chain increased. Generally, increasing the alkyl chain increases the mesomorphic range ($\Delta T=T_i-T_m$). Therefore, ΔT of N4 should have been higher than N2; however, the DSC results showed the opposite trend. The reason for this trend is unclear. The results from the DSC analysis were further supported by the POM analysis. Both gelators exhibited grainy nematic liquid crystalline phases under heating and cooling cycles. For example, the representative POM textures of N4 during heating and cooling cycles are shown in Fig**. 9**. The initial grainy texture of N4 (at 120 °C) became nematic when the temperature increased to 190 °C and then become isotropic at 200 °C. During the cooling cycle, a grainy nematic texture was observed at 170 °C, and the sample crystallized at 125 °C. Since the cholesteryl group is attached to this gelator molecule, a cholesteric or chiral nematic mesophase was expected, but no clear images were observed to support the phenomenon. This may have been due to the highly rigid rod-like structure of the gelator molecules, indicating that the flexibility given by 2 and 4 carbon long alkyl chains was not sufficient to widening the liquid crystalline phase. Moreover, if the alkyl chain length is increased, then it will lose its gelation ability, as stated in our previous report[30, 54]; gelators with linkers 6 carbons long had high CGC values, and gelators with linkers 11 carbons long failed to form gels.

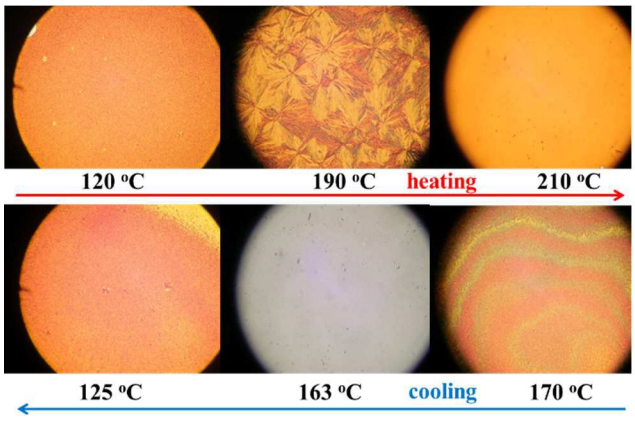

Fig. 9 Selected POM textures of N4 at different temperatures (heating and cooling cycles) at a magnification of 10X.

From an application point of view, these gelators can act as phase-selective gelators[74] that can be useful for the separation of solvents. Since the gelator molecules selectively gel one solvent over anther, the nongelling solvent can easily be separated by filtration and purified by distillation. For example, approximately 5 mg of gelator N4 was added to 0.4 ml of a mixture of solvents, such as xylene/water and DMSO/hexane (1:1 ratios), and stirred vigorously. One gelling and one nongelling solvent were chosen for the preparation of the solvent mixtures for this process. Then, the resulting mixture was subjected to heating and cooling to make the system homogeneous and improve the solubility of the gelator. N4 gelled only one solvent in each mixture; for example N4 selectively gelled only xylene, and the water was removed by filtration. Similarly, N4 gelled DMSO, allowing the hexane to be recovered by filtration, as shown in **Fig. 10**. These solvents were further purified by distillation. The xylene and DMSO in the gels could be extracted by isomerization followed by vacuum distillation since the irradiation of the gels by UV light resulted in the irreversible gel→ sol transition. Therefore, the solvent can be recovered by vacuum distillation. In this way, we can separate the solvents (gelling and nongelling solvents) from the solvent mixtures.

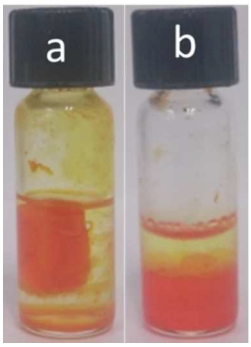

Fig. 10. Selective gelation of N4 from (a) a xylene/water mixture and (b) a DMSO/hexane mixture.

Conclusions

In conclusion, two azobenzene derivatives (N2 and N4) with different spacer lengths were synthesized, and their gelation abilities in a variety of solvents were studied. Of the two, N4 acted as a more versatile gelator than N2. The morphological, thermal and optical properties of N2 and N4 were studied with respect to alkyl chain length. The morphological studies revealed that N2 formed spherical nanoparticles, whereas N4 self-assembled into fibers. It was found that the π-π stacking of the aromatic units and intermolecular forces, such as van der Waals forces and hydrogen bonding, played important roles and acted as driving forces for the self-assembly. This behavior is supported by the temperature dependent ^{1}H-NMR, FT-IR, and XRD analyses along with the results from simulation software. The photolysis of N2 and N4 revealed that N2 and N4 underwent *trans*-to-*cis* isomerization by UV light that caused a gel→sol transition; however, the gel state could not be recovered using visible light since the *cis*-conformation was more stable. Hence, the gel state could be retained by further heating and cooling of the *cis*-form. Both gelators exhibited grainy nematic mesophase textures according to the POM analysis, which was supported by the DSC analysis. In addition, these gelators underwent phase-selective gelation, which adds more value to these gelators due to their ability to separate solvents.

View Article Online
DOI: 10.1039/C7NJ03059B

Notes and references

[a] *Department of Chemical Engineering, National Cheng Kung University, Tainan 70101, Taiwan, Republic of China*. Fax: +886-6- 2384590; Tel.: +886-6-2757575ext.62646; Corresponding author E-mail: jhliu@mail.ncku.edu.tw

† Electronic Supplementary Information (ESI) available: Experimental and characterization details of the compounds and DSC analyses of the compounds. DOI: 10.1039/b000000x/.

The authors thank the Ministry of Science and Technology (MOST) of the Republic of China (Taiwan) for financially supporting this research under Contract nos. MOST 105-2923-E-006-007 and MOST 104-2923-E-006 -004 -MY3.

1. X. Y. Hou, D. Gao, J. L. Yan, Y. Ma, K. Q. Liu and Y. Fang, *Langmuir*, 2011, **27**, 12156-12163.
2. A. Ajayaghosh, V. K. Praveen and C. Vijayakumar, *Chemical Society Reviews*, 2008, **37**, 109-122.
3. A. Ajayaghosh and V. K. Praveen, *Accounts of Chemical Research*, 2007, **40**, 644-656.
4. A. Aggeli, M. Bell, N. Boden, J. N. Keen, P. F. Knowles, T. C. B. McLeish, M. Pitkeathly and S. E. Radford, *Nature*, 1997, **386**, 259-262.
5. H. Ihara, T. Sakurai, T. Yamada, T. Hashimoto, M. Takafuji, T. Sagawa and H. Hachisako, *Langmuir*, 2002, **18**, 7120-7123.
6. T. Naota and H. Koori, *Journal of the American Chemical Society*, 2005, **127**, 9324-9325.
7. G. Zhu and J. S. Dordick, *Chemistry of Materials*, 2006, **18**, 5988-5995.
8. C. C. Chien and J. H. Liu, *Science of Advanced Materials*, 2014, **6**, 111-119.
9. R. Xing, K. Liu, T. Jiao, N. Zhang, K. Ma, R. Zhang, Q. Zou, G. Ma and X. Yan, *Advanced Materials*, 2016, **28**, 3669-3676.
10. X. Zhao, K. Ma, T. Jiao, R. Xing, X. Ma, J. Hu, H. Huang, L. Zhang and X. Yan, 2017, **7**, 44076.
11. K. Sugiyasu, N. Fujita and S. Shinkai, *Angewandte Chemie International Edition*, 2004, **43**, 1229-1233.
12. Y. Wu, S. Wu, X. Tian, X. Wang, W. Wu, G. Zou and Q. Zhang, *Soft Matter*, 2011, **7**, 716-721.
13. R. Perez-Ruiz and D. Diaz Diaz, *Soft Matter*, 2015, **11**, 5180-5187.
14. H. C. Lim, S. H. Min, E. Lee, J. Jang, S. H. Kim and J.-I. Hong, *ACS Applied Materials & Interfaces*, 2015, **7**, 11069-11073.
15. M. M. Ibrahim, S. A. Hafez and M. M. Mahdy, *Asian Journal of Pharmaceutical Sciences*, 2013, **8**, 48-57.
16. Y. Meng and Y. Yang, *Electrochemistry Communications*, 2007, **9**, 1428-1433.
17. S. Chen, X. Q. Tong, H. W. He, M. Ma, Y. Q. Shi and X. Wang, *Acs Applied Materials & Interfaces*, 2017, **9**, 11924-11932.
18. P. Deindorfer, R. Davis and R. Zentel, *Soft Matter*, 2007, **3**, 1308-1311.
19. T. Haino, Y. Hirai, T. Ikeda and H. Saito, *Organic & Biomolecular Chemistry*, 2013, **11**, 4164-4170.
20. T. F. Jiao, Y. J. Wang, Q. R. Zhang, J. X. Zhou and F. M. Gao, *Nanoscale Research Letters*, 2013, **8**.
21. J. H. Jung, S. H. Lee, J. S. Yoo, K. Yoshida, T. Shimizu and S. Shinkai, *Chemistry-a European Journal*, 2003, **9**, 5307-5313.
22. H. Kobayashi, A. Friggeri, K. Koumoto, M. Amaike, S. Shinkai and D. N. Reinhoudt, *Organic Letters*, 2002, **4**, 1423-1426.
23. A. Pal, S. Shrivastava and J. Dey, *Chemical Communications*, 2009, DOI: 10.1039/b914665b, 6997-6999.
24. X. Ran, L. L. Shi, K. Zhang, J. Lou, B. Liu and L. J. Guo, *Journal of Nanomaterials*, 2015, DOI: 10.1155/2015/357875.
25. R. M. Yang, S. H. Peng and T. C. Hughes, *Soft Matter*, 2014, **10**, 2188-2196.
26. J. Wu, T. Yi, Q. Xia, Y. Zou, F. Liu, J. Dong, T. Shu, F. Li and C. Huang, *Chemistry – A European Journal*, 2009, **15**, 6234-6243.
27. M. Žinić, F. Vögtle and F. Fages, *Journal*, 2005, **256**, 39-76.
28. T. Jiao, Y. Wang, F. Gao, J. Zhou and F. Gao, *Progress in Natural Science: Materials International*, 2012, **22**, 64-70.
29. C. Baddeley, Z. Q. Yan, G. King, P. M. Woodward and J. D. Badjic, *Journal of Organic Chemistry*, 2007, **72**, 7270-7278.
30. R. Balamurugan, Y. S. Zhang, S. Fitriyani and J. H. Liu, *Soft Matter*, 2016, **12**, 5214-5223.
31. T. F. Jiao, F. Q. Gao, X. H. Shen, Q. R. Zhang, X. F. Zhang, J. X. Zhou and F. M. Gao, *Materials*, 2013, **6**, 5893-5906.
32. S. Kawano, N. Fujita and S. Shinkai, *Chemistry-a European Journal*, 2005, **11**, 4735-4742.
33. P. Terech, I. Furman, R. G. Weiss, H. BouasLaurent, J. P. Desvergne and R. Ramasseul, *Faraday Discussions*, 1995, **101**, 345-358.
34. Y. P. Zhang, Y. Ma, M. Y. Deng, H. X. Shang, C. S. Liang and S. M. Jiang, *Soft Matter*, 2015, **11**, 5095-5100.
35. M. Zinic, F. Vogtle and F. Fages, in *Low Molecular Mass Gelators: Design, Self-Assembly, Function*, ed. F. Fages, 2005, vol. 256, pp. 39-76.
36. B. L. Bai, X. Y. Mao, J. Wei, Z. H. Wei, H. T. Wang and M. Li, *Sensors and Actuators B-Chemical*, 2015, **211**, 268-274.
37. B. L. Bai, M. G. Zhang, J. Wei, H. Y. Yan, H. T. Wang, Y. Q. Wu and M. Li, *Tetrahedron*, 2016, **72**, 5363-5368.
38. S. Balamurugan, G. Y. Yeap, W. A. K. Mahmood, P. L. Tan and K. Y. Cheong, *Journal of Photochemistry and Photobiology a-Chemistry*, 2014, **278**, 19-24.
39. X. H. Cao, X. Liu, L. M. Chen, Y. Y. Mao, H. C. Lan and T. Yi, *Journal of Colloid and Interface Science*, 2015, **458**, 187-193.
40. P. F. Duan, Y. G. Li, L. C. Li, J. G. Deng and M. H. Liu, *Journal of Physical Chemistry B*, 2011, **115**, 3322-3329.
41. X. J. Gu, B. L. Bai, H. T. Wang and M. Li, *Rsc Advances*, 2017, **7**, 218-223.
42. H. Y. Guo, T. F. Jiao, X. H. Shen, Q. R. Zhang, A. D. Li and F. M. Gao, *Journal of Spectroscopy*, 2014, DOI: 10.1155/2014/758765.
43. Y. M. Hu, Q. S. Li, W. Hong, T. F. Jiao, G. Z. Xing and Q. L. Jiang, *Journal of Spectroscopy*, 2014, DOI: 10.1155/2014/970827.
44. T. Ishi-i and S. Shinkai, in *Supermolecular Dye Chemistry*, ed. F. Wurthner, 2005, vol. 258, pp. 119-160.
45. T. F. Jiao, Y. J. Wang, F. Q. Gao, J. X. Zhou and F. M. Gao, *Progress in Natural Science-Materials International*, 2012, **22**, 64-70.
46. M. Kurita, M. Makihara and H. Nakano, *Soft Materials*, 2014, **12**, 42-46.
47. Z. Y. Li, Y. D. Huang, D. L. Fan, H. M. Li, S. X. Liu and L. Y. Wang, *Frontiers of Chemical Science and Engineering*, 2016, **10**, 552-561.
48. G. Palui and A. Banerjee, *Journal of Physical Chemistry B*, 2008, **112**, 10107-10115.
49. X. Ran, H. T. Wang, P. Zhang, B. L. Bai, C. X. Zhao, Z. X. Yu and M. Li, *Soft Matter*, 2011, **7**, 8561-8566.
50. Y. C. Ren, B. Wang and X. Q. Zhang, *Beilstein Journal of Organic Chemistry*, 2015, **11**, 1089-1095.
51. M. Suzuki, Y. Maruyama and K. Hanabusa, *Tetrahedron Letters*, 2016, **57**, 3540-3543.
52. Y. P. Wu, S. Wu, G. Zou and Q. J. Zhang, *Soft Matter*, 2011, **7**, 9177-9183.
53. Y. F. Zhou, M. Xu, J. C. Wu, T. Yi, J. T. Han, S. Z. Xiao, F. Y. Li and C. H. Huang, *Journal of Physical Organic Chemistry*, 2008, **21**, 338-343.
54. R. Balamurugan, W. Kai-Ming, C.-C. Chien and J. H. Liu, *Soft Matter*, 2014, **10**, 8963-8970.
55. M. F. Rizkiana, R. Balamurugan and J. H. Liu, *New Journal of Chemistry*, 2015, **39**, 6068-6075.
56. S. K. Choi, T. P. Thomas, M.-H. Li, A. Desai, A. Kotlyar and J. R. Baker, *Photochemical & photobiological sciences : Official journal of the European Photochemistry Association*

View Article Online
DOI: 10.1039/C7NJ03059B

and the European Society for Photobiology, 2012, **11**, 653-660.
57. R. Balamurugan, W. Kai-Ming, C. C. Chien and J. H. Liu, *Soft Matter*, 2014, **10**, 8963-8970.
58. H. Guo, T. Jiao, Q. Zhang, W. Guo, Q. Peng and X. Yan, *Nanoscale Research Letters*, 2015, **10**, 272.
59. J. Liu, K. Zhu, T. Jiao, R. Xing, W. Hong, L. Zhang, Q. Zhang and Q. Peng, *Colloids and Surfaces A: Physicochemical and Engineering Aspects*, 2017, **529**, 668-676.
60. S. Banerjee, R. K. Das and U. Maitra, *Journal of Materials Chemistry*, 2009, **19**, 6649-6687.
61. F. Aparicio, S. Cherumukkil, A. Ajayaghosh and L. Sanchez, *Langmuir*, 2016, **32**, 284-289.
62. S. S. Babu, K. K. Kartha and A. Ajayaghosh, *Journal of Physical Chemistry Letters*, 2010, **1**, 3413-3424.
63. S. S. Babu, S. Prasanthkumar and A. Ajayaghosh, *Angewandte Chemie-International Edition*, 2012, **51**, 1766-1776.
64. S. S. Babu, V. K. Praveen and A. Ajayaghosh, *Chemical Reviews*, 2014, **114**, 1973-2129.
65. S. Ghosh, V. K. Praveen and A. Ajayaghosh, in *Annual Review of Materials Research, Vol 46*, ed. D. R. Clarke, 2016, vol. 46, pp. 235-262.
66. A. Gopal, R. Varghese and A. Ajayaghosh, *Chemistry-an Asian Journal*, 2012, **7**, 2061-2067.
67. R. D. Mukhopadhyay and A. Ajayaghosh, *Science*, 2015, **349**, 241-242.
68. R. D. Mukhopadhyay, V. K. Praveen and A. Ajayaghosh, *Materials Horizons*, 2014, **1**, 572-576.
69. S. Prasanthkumar, A. Gopal and A. Ajayaghosh, *Journal of the American Chemical Society*, 2010, **132**, 13206-13207.
70. A. Ajayaghosh and V. K. Praveen, *Accounts of Chemical Research*, 2007, **40**, 644-656.
71. A. Ajayaghosh, V. K. Praveen, S. Srinivasan and R. Varghese, *Advanced Materials*, 2007, **19**, 411-+.
72. V. K. Praveen, S. J. George and A. Ajayaghosh, *Macromolecular Symposia*, 2006, **241**, 1-8.
73. R. Xing, T. Jiao, Y. Liu, K. Ma, Q. Zou, G. Ma and X. Yan, *Polymers*, 2016, **8**, 181.
74. R. Rajaganesh, A. Gopal, T. Mohan Das and A. Ajayaghosh, *Organic Letters*, 2012, **14**, 748-751.

View Article Online
DOI: 10.1039/C7NJ03059B

Graphical Abstract

Dual-responsive ALS-type organogelators based on azobenzene-cholesteryl conjugates and their self-assemblies

Sheng-Yang Kuo[1], Chun-Yen Liu[2], Rathinam Balamurugan[1], Yan-Song Zhang[1], Sri Fitriyani[1] and Jui Hsiang Liu[1]*

[1] *Department of Chemical Engineering, National Cheng Kung University, Tainan70101, Taiwan, Republic of China*. Fax: +886-6- 2384590; Tel: +886-6-2757575ext.62646 Corresponding author E-mail: jhliu@mail.ncku.edu.tw

[2] *School of Optometry and Vision Science Program, UC Berkeley, Berkeley, CA 94720, USA*

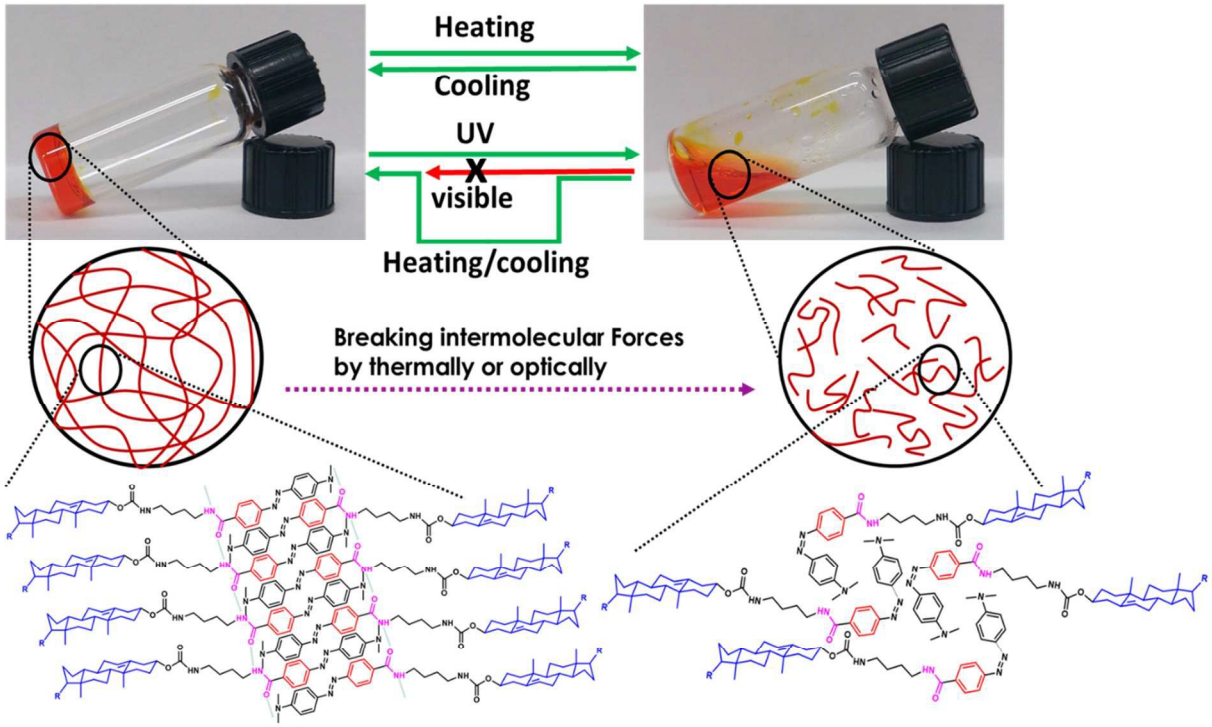

The azobenzene and cholesteryl based derivatives (N2 and N4) were designed as gelators and their aggregation mechanism is proposed. These gelators are thermally reversible, however optically irreversible. Hence gel state was retained by further treatment with heating and cooling process. These gelators undergo phase-selective gelation which added more value to these gelators in the aspect of separation/purification of solvents.